Spatiotemporal vortices in optical fiber bundles

Hervé Leblond,[1] Boris A. Malomed,[2] and Dumitru Mihalache[3]
[1]*Laboratoire POMA, FRE 2988, Université d'Angers, 2 Bd Lavoisier, 49000 Angers, France*
[2]*Department of Interdisciplinary Studies, School of Electrical Engineering, Faculty of Engineering, Tel Aviv University, Tel Aviv 69978, Israel*
[3]*Department of Theoretical Physics, Horia Hulubei National Institute for Physics and Nuclear Engineering, 407 Atomistilor, Magurele-Bucharest 077125, Romania*
(Received 29 November 2007; published 5 June 2008)

We analyze complex spatiotemporal semidiscrete solitons in a model of a set of nonlinear optical fibers which form a square lattice in the cross section. The medium was recently realized as a set of parallel waveguides written in fused silica. The model also applies to a self-attracting Bose-Einstein condensate trapped in a very strong quasi-two-dimensional optical lattice. By means of the variational approximation (VA) and using numerical methods, we construct several species of the semidiscrete solitons, including vortices of rhombus (alias cross) and square types, with vorticity $S=1$ and 2, and quadrupoles. The VA is developed for narrow cross vortices with $S=1$ and quadrupoles, which turn out to be the most stable species. Two finite stability intervals are also found for the square-shaped vortices with $S=1$, while all the vortices with $S=2$ are unstable. For the unstable solitons, several scenarios of the instability development are identified, such as fusion of the entire complex into a single fundamental soliton, or splitting into coherent soliton pairs.

DOI: 10.1103/PhysRevA.77.063804 PACS number(s): 42.65.Tg, 42.81.Dp, 03.75.Lm, 05.45.Yv

I. INTRODUCTION

Experimental and theoretical studies of spatial solitons in discrete and quasidiscrete media represent an essential part of the current developments in nonlinear optics. A paradigmatic model of such media is provided by the discrete nonlinear Schrödinger (DNLS) equation [1]. A realization of the one-dimensional (1D) DNLS model with the cubic (Kerr) onsite nonlinearity in arrays of optical waveguides was predicted in Ref. [2]. This prediction was implemented in an array of parallel semiconductor waveguides built on a common substrate, and in arrays of optical fibers [3]. In addition to the permanent structures, quasidiscrete multicore waveguiding systems can be also be created in a virtual form, as photonic lattices in photorefractive crystals [4] (in that case, the nonlinearity is saturable, rather than cubic). The latter technique made it possible to create two-dimensional (2D) discrete solitons [5], vortex solitons in the same setting [6] (localized lattice states with vorticity, alias "spin," $S=1$ were predicted in Ref. [7], and higher-order vortices, with $S>1$, and multipole solitons were studied in Ref. [8]), lattice solitons in the second band gap [9], stable necklace patterns [10], and other structures. Recently, the creation of 2D spatial solitons was reported [11] in a bundle of fiberlike waveguides (of transverse size 5×5), permanently written in bulk silica by means of a technique using femtosecond laser pulses shone onto the bulk sample in the perpendicular direction [12]. Another medium which may serve as a carrier for quasidiscrete 2D solitons are photonic-crystal fibers; in particular, spatial vortex solitons were predicted in them [13].

Also investigated, theoretically and experimentally, were various nonstationary effects (chiefly, in 1D arrays), such as the mobility [14,15] and collisions of discrete solitons [15,16], and onset of the spatiotemporal collapse in an array of self-focusing waveguides [17]. In addition to the optical settings, it has also been demonstrated that the DNLS equation with the cubic nonlinearity is an adequate model for the Bose-Einstein condensate (BEC) trapped in a deep optical lattice, which effectively splits the condensate into a set of "droplets" captured in local potential wells and coupled linearly by tunneling of atoms [18]. Still another physical realization of this model is offered by crystals built of microscopic cavities trapping photons or polaritons [19].

A majority of the above-mentioned works were dealing with the spatial-domain dynamics in 1D or 2D arrays. Indeed, photonic lattices in photorefractive crystals do not allow one to study the temporal dynamics along the direction of the propagation of the probe beam, as the response time of the medium is very large. On the other hand, a system built as a planar (1D) set of parallel optical fibers with the intrinsic Kerr nonlinearity suggests a possibility to consider an interplay of the continuous temporal dynamics along the fibers' axes and discrete evolution in the transverse direction. In that context, spatiotemporal semidiscrete solitons ("light bullets") [20], self-compression of pulses under the action of the quasicollapse [21], steering of the pulses [22], and various aspects of the modulational instability [23] were analyzed theoretically. Spatiotemporal optical solitons [24] in models of waveguiding arrays with the quadratic (rather than Kerr) nonlinearity were studied too [25]. Recently, semidiscrete spatiotemporal solitons were considered in models of waveguide arrays with an edge (surface) [26], and with an interface between two different arrays [27]. In the latter case, solitons of a combined staggered-unstaggered type have been found (in Ref. [28], evidence was given for the existence of such hybrid modes, in the form of discrete spatial solitons). Spatiotemporal light localization in truncated two-dimensional photonic lattices was considered also [29].

The availability of bundled (two-dimensional) arrays of long fiberlike waveguides written in fused silica [11,12] suggests a possibility to consider 3D spatiotemporal solitons, continuous along the axis of the bundle, and discrete in the

two transverse directions. The same solutions should apply to the description of matter-wave solitons in a self-attractive BEC trapped in a quasi-2D optical lattice [30], in the limit case of a very strong lattice. The objective of the present work is to study solitons of this type with intrinsic vorticity, and also solitons of the quadrupole type, which are more interesting than plain fundamental solitons. It is relevant to mention that vortex solitons in a continuum counterpart of this model, based on the three-dimensional (3D) NLS equation with a 2D periodic potential, were recently investigated in Ref. [31], where families of stable localized states with vorticity $S=1$ and 2 were found, by means of the variational approximation (VA) and numerical methods. As concerns the full DNLS equation in three dimensions, various families of vortex-soliton states in it were reported in Ref. [32].

The paper is organized as follows. The model and the VA for some types of the semidiscrete vortex and quadrupole solitons supported by the model are formulated in Sec. II. In Sec. III, numerical results are reported for vortices of the "rhombus" (alias "cross") type with $S=1$ (they contain an empty site at the center). These solitons are stable if they are sufficiently narrow, i.e., if the corresponding propagation constant, μ, is large enough; in that case, their shape is accurately predicted by the VA. Numerical results for vortex solitons of another, "square" type (with the center set between the sites, hence there is no empty site in the middle) are presented in Sec. IV. Unlike their cross-shaped counterparts, these vortical solitons are stable in two finite intervals of μ. Section V is dealing with vortices of both types (rhombus- and square-shaped) with $S=2$, which are found to be always unstable, but, in some cases, the development of their instability may lead to interesting effects. Finally, in Sec. VI we consider quadrupole solitons, which carry zero vorticity, but feature a nontrivial intrinsic structure. Unlike the unstable vortices with $S=2$, the quadrupoles are definitely stable for large μ, and even when they are unstable (typically, merging into a single fundamental soliton, or splitting into two pairs of coherently coupled solitons), they feature very slow development of the instability, i.e., the quadrupoles appear to be remarkably robust objects. The paper is concluded by Sec. VI.

II. FORMULATIONS

A. Model

The system of evolution equations for local amplitudes of the electromagnetic waves in the bundle of fiber waveguides with the square-grid cross section, $u_{m,n}(\tau)$, are obtained as a straightforward generalization of the respective model for a planar fiber array [20–23],

$$i\frac{\partial u_{m,n}}{\partial z}-\frac{1}{2}\beta\frac{\partial^2 u_{m,n}}{\partial \tau^2}+|u_{m,n}|^2u_{m,n}+C(u_{m+1,n}+u_{m-1,n}+u_{m,n+1}+u_{m,n-1}-4u_{m,n})=0. \tag{1}$$

Here (m,n) are discrete coordinates of the core belonging to the array, $C>0$ is a real coupling constant, that may be scaled to be +1 (in the bundled array of waveguides written in bulk silica, the corresponding coupling length, $\sim 1/C$, may be on the order of several centimeters [11,12]), continuous variable τ is the usual reduced time and β the group-velocity-dispersion (GVD) coefficient [33]. We assume the anomalous GVD, $\beta<0$ (otherwise, solitons cannot exist in the temporal direction), and normalize it by fixing $\beta\equiv -1$. Thus, the scaled equations become

$$i\frac{\partial u_{m,n}}{\partial z}+\frac{1}{2}\frac{\partial^2 u_{m,n}}{\partial \tau^2}+|u_{m,n}|^2u_{m,n}+(u_{m+1,n}+u_{m-1,n}+u_{m,n+1}+u_{m,n-1}-4u_{m,n})=0. \tag{2}$$

BEC loaded into a very strong quasi-2D optical lattice is described by a system of linearly coupled Gross-Pitaevskii equations for the mean-field wave functions of condensates trapped in individual "potential tubes" induced by the lattice. As follows from the analysis presented in Ref. [18], in the simplest approximation (for sufficiently low atomic density) the coupled system is tantamount, in the normalized form, to Eq. (2), with z replaced by time, and τ replaced by the longitudinal coordinate.

Families of stationary solutions to Eq. (2), parametrized by propagation constant μ, are looked for as $u_{m,n}(z,\tau)=e^{i\mu z}U_{m,n}(\tau)$, with functions $U_{m,n}$ obeying a system of linearly coupled ordinary differential equations,

$$\frac{1}{2}\frac{d^2U_{m,n}}{d\tau^2}+|U_{m,n}|^2U_{m,n}+(U_{m+1,n}+U_{m-1,n}+U_{m,n+1}+U_{m,n-1})=(4+\mu)U_{m,n}. \tag{3}$$

B. Basic types of vortex solitons

The definition of the vortex requires the phase of complex field $U_{m,n}$ to change by $2\pi S$, with $S=1,2,3,\ldots$, as a result of a round trip around the center of the vortex. In the experiment, the vorticity may be imparted to the optical soliton by passing a broad (but sufficiently short, in the temporal direction) laser beam, which is coupled into the fiber bundle, through a properly designed phase plate [34]. In the application to the BEC, the vorticity may be transferred to the condensate from a laser beam, as was predicted, in various forms, theoretically [35] and demonstrated experimentally [36].

For continuous-wave (cw, i.e., τ-independent) solutions, Eq. (3) reduce to algebraic equations,

$$|U_{m,n}|^2U_{m,n}+(U_{m+1,n}+U_{m-1,n}+U_{m,n+1}+U_{m,n-1})=(4+\mu)U_{m,n}. \tag{4}$$

Fundamental localized vortex solutions to Eq. (4) (with $S=1$) were found in Ref. [7]. It was concluded that there is a critical value $P_{\rm cr}$ of the total power, $P=\Sigma_{m,n}|U_{m,n}|^2$, and a respective critical wave number, $\mu_{\rm cr}\approx 2.46$, such that the cw vortices with $P>P_{\rm cr}$ and $\mu>\mu_{\rm cr}$ are stable as solutions to Eqs. (1) with $\beta=0$, and unstable otherwise. Higher-order cw vortices with $S=2$ are completely unstable, but ones with $S=3$, as well as quadrupoles, have their stability regions [8].

Following the analysis of the localized states in the 2D lattice [8], and of similar solutions in the continuum coun-

terpart of the model (the 2D NLS equation with a checkerboard periodic potential) [37], we expect that the semidiscrete vortex solitons may be of two different types, *viz.*, "rhombuses" (alias "crosses") and "squares." The former one with $S=1$ is based on the frame ("skeleton") composed of four lattice sites, with coordinates

$$(m,n) = (1,0),(0,1),(-1,0),(0,-1), \tag{5}$$

while the central site, at $(m,n)=(0,0)$, remains empty. The respective cross-vortex solutions to Eq. (3) can be found starting, in the anticontinuum limit [which corresponds to $C\to 0$ in Eq. (1)], with an initial guess which emulates frame (5),

$$(U^{(\mathrm{X})}_{1,0})_0 = -(U^{(\mathrm{X})}_{-1,0})_0 = U_{\mathrm{sol}}(\tau),$$

$$(U^{(\mathrm{X})}_{0,1})_0 = -(U^{(\mathrm{X})}_{0,-1})_0 = iU_{\mathrm{sol}}(\tau), \tag{6}$$

$$U_{\mathrm{sol}}(\tau) = \eta\,\mathrm{sech}(\eta\tau), \quad \eta^2 = 2(4+\mu), \tag{7}$$

and $(U^{(\mathrm{X})}_{m,n})_0 \equiv 0$ at all other sites, including (0,0). The choice of the τ dependence in Eq. (7) corresponds to the ordinary temporal soliton in the single core, with amplitude η corresponding to effective propagation constant $4+\mu$, in the absence of the linear coupling between adjacent cores.

The difference of the "square"-shaped vortices is that they do not include an empty site at the center, placing the "virtual" pivot of the vortex between lattice sites. Accordingly, the frame for the square vortex with $S=1$ is composed of four sites with coordinates

$$(m,n) = (0,0),(1,0),(1,1),(0,1), \tag{8}$$

cf. Eq. (5). The simplest initial guess for constructing the respective semidiscrete square-vortex soliton is based on the following set of nonzero elements:

$$(U^{(\mathrm{Sq})}_{0,0})_0 = -(U^{(\mathrm{Sq})}_{1,1})_0 = U_{\mathrm{sol}}(\tau),$$

$$(U^{(\mathrm{Sq})}_{0,1})_0 = -(U^{(\mathrm{Sq})}_{1,0})_0 = iU_{\mathrm{sol}}(\tau), \tag{9}$$

with the same $U_{\mathrm{sol}}(\tau)$ as in Eq. (7).

C. Variational approximation

To develop the VA for stationary solutions, we note that Eq. (3) can be derived from the following Lagrangian:

$$L = \sum_{m,n=-\infty}^{+\infty} \int_{-\infty}^{+\infty} d\tau \mathcal{L}_{m,n}(\tau),$$

$$\mathcal{L}_{m,n} = -\frac{1}{2}\left|\frac{dU_{m,n}}{d\tau}\right|^2 + \frac{1}{2}|U_{m,n}|^4 + \{U^*_{m,n}(U_{m,n-1}+U_{m-1,n}) + \mathrm{c.c.}\} - (4+\mu)|U_{m,n}|^2, \tag{10}$$

where c.c. and asterisk both stand for the complex conjugation. For vortex solitons of the cross or rhombus ("X") type, with $S=1$, we adopt the following *ansatz*, suggested by the general pattern of the VA developed for 1D discrete solitons in Ref. [38], and for fundamental (zero-vorticity) 2D solitons in Ref. [39]:

$$(U^{(\mathrm{X})}_{m,n})_{\mathrm{ansatz}} = A\frac{(m+in)e^{-a(|m|+|n|)}}{\cosh(\eta\tau)}, \tag{11}$$

cf. Eqs. (6) and (7), where A, a, and η are real variational parameters. The substitution of ansatz (11) in Eq. (10) leads to a very cumbersome expression, in the general case. However, it becomes tractable in the limit case of a narrow (compact) vortex soliton, with $e^{-a}\ll 1$, which is the case for stable vortex solitons, see below,

$$L^{(\mathrm{X})}_{\mathrm{eff}} \approx 16\frac{B}{\eta}e^{-a} - B\left(\frac{1}{3}\eta + \frac{2}{\eta}(4+\mu)\right)(1+6e^{-2a}) + \frac{B^2}{6\eta},$$

$$B \equiv 4A^2e^{-2a}. \tag{12}$$

Actually, expression (12) takes into account contributions from the lattice sites with $|m|+|n|\le 2$. Note that terms $\sim e^{-a}$ and e^{-2a} in this effective Lagrangian are small corrections to terms that do not explicitly contain e^{-a}, but they should be kept, otherwise the variation of the Lagrangian in a cannot be performed.

The variational equations following from Eq. (12), $\partial L_{\mathrm{eff}}/\partial B = \partial L_{\mathrm{eff}}/\partial\eta = \partial L_{\mathrm{eff}}/\partial(e^{-a}) = 0$, yield the following results, for the vortex soliton of the cross or rhombus type:

$$\eta^2_{\mathrm{X}} = 2(4+\mu), \quad B_{\mathrm{X}} = 8(4+\mu), \quad \exp(a_{\mathrm{X}}) = 2(4+\mu) \tag{13}$$

[note the first equality is tantamount to the usual relation between the amplitude and propagation constant of the single-core temporal soliton, cf. Eq. (7)]. The last relation in Eq. (13) implies that the above assumption, $e^{-a}\ll 1$, holds for $\mu\gtrsim 1$ (the actual stability region for the cross-shaped vortices is $\mu\gtrsim 19$, as shown below, hence the stable vortex solitons of this type are definitely narrow ones).

In the same approximation, $e^{-a}\ll 1$, the total energy of the vortex soliton is

$$E \equiv \sum_{m,n=-\infty}^{+\infty} \int_{-\infty}^{+\infty} d\tau |U_{m,n}(\tau)|^2 \approx 8\sqrt{2(4+\mu)}. \tag{14}$$

Note that expression (14) satisfies the Vakhitov-Kolokolov stability criterion, $dE/d\mu > 0$ [40]. For soliton solutions of equations of the NLS type with self-focusing nonlinearity, this condition is necessary, but not sufficient, for the stability, as it may guarantee the absence of unstable real eigenvalues in the spectrum of small perturbations around the soliton, but it cannot detect complex eigenvalues, that may account for an oscillatory instability [41]. In particular, vortex solitons are frequently subject to the instability of the latter type, which tends to split the vortex into a set of fundamental (zero-vorticity) pulses [24].

It is relevant to compare the above variational solution to its cw counterpart for the localized cross-shaped vortex (with $S=1$) known in the ordinary 2D-lattice model, without the τ dependence [1]. To this end, one may take Lagrangian (12) in the limit of $\eta\to 0$,

$$(L_{\rm eff}^{(\rm X)})_{\rm cw} \equiv \lim_{\eta\to 0}(\eta L_{\rm eff}^{(\rm X)})$$

$$\approx 16Be^{-a} - 2B(4+\mu)(1+6e^{-2a}) + \frac{B^2}{6}. \quad (15)$$

The respective variational equations, $\partial L_{\rm eff}/\partial B = \partial L_{\rm eff}/\partial(e^{-a}) = 0$, yield the following results, to be compared with Eqs. (13):

$$B_{\rm cw}^{(\rm X)} = 6(4+\mu), \quad \exp(a_{\rm cw}^{(\rm X)}) = \frac{3}{2}(4+\mu). \quad (16)$$

Another relatively simple variational ansatz can be devised for a semidiscrete solution in the form of a quadrupole soliton, which is a structured localized state with zero vorticity [8],

$$(U_{m,n}^{(\rm Q)})_{\rm ansatz} = A\frac{(m^2-n^2)e^{-a(|m|+|n|)}}{\cosh(\eta\tau)}. \quad (17)$$

Note that this expression is real, unlike the complex one for the vortex, see Eq. (11), and it corresponds to the "frame" coinciding with the one given by Eq. (5) for the cross-vortex soliton with $S=1$. Substituting ansatz (17) in Eq. (10), and again assuming a compact pattern ($e^{-a} \ll 1$), i.e., constraining the summation to $|m|+|n| \le 2$, we derive the following effective Lagrangian, cf. Eq. (12):

$$L_{\rm eff}^{(\rm Q)} \approx 16\frac{B}{\eta}e^{-a} - \left(\frac{1}{3}\eta + \frac{2}{\eta}(4+\mu)\right)B(1+16e^{-2a}) + \frac{B^2}{6\eta}, \quad (18)$$

where B is the same as above. The variational equations which follow from this Lagrangian yield the following results:

$$\eta_{\rm Q}^2 = 2(4+\mu), \quad B_{\rm Q} = 8(4+\mu), \quad \exp(a_{\rm Q}) = \frac{16}{3}(4+\mu), \quad (19)$$

cf. solution (13) for the cross-shaped vortex soliton. Note that assumption $e^{-a} \ll 1$ definitely holds for stable quadrupoles, whose stability region is $\mu \gtrsim 20$, see below. In the lowest approximation, the total energy of the quadrupole soliton is given by the same expression, Eq. (14), as above.

To compare these results with those for the quadrupole soliton in the ordinary (cw) 2D lattice, we note that the corresponding effective Lagrangian is [cf. Eq. (15)]

$$(L_{\rm eff}^{(\rm Q)})_{\rm cw} \equiv \lim_{\eta\to 0}(\eta L_{\rm eff}^{(\rm Q)})$$

$$\approx 16Be^{-a} - 2B(4+\mu)(1+16e^{-2a}) + \frac{B^2}{6}.$$

The variational equations following from this Lagrangian yield

$$B_{\rm cw}^{(\rm Q)} = 6(4+\mu), \quad \exp(a_{\rm cw}^{(\rm Q)}) = 14(4+\mu), \quad (20)$$

cf. Eqs. (16) and (19).

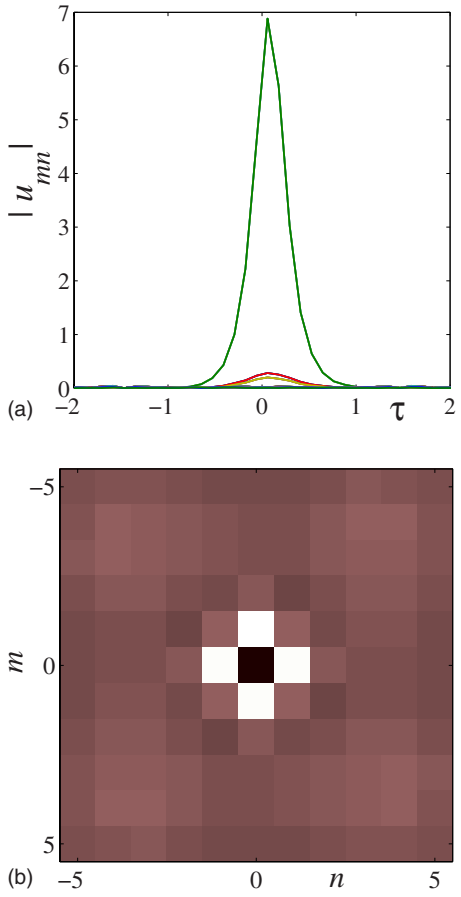

FIG. 1. (Color online) An example of a stable vortex soliton of the cross (alias rhombus) type, which self-traps from initial configuration (11) with $\mu=20$ (stable vortex solitons of this type are generated with $\mu \ge \mu_{\rm cr} \approx 19$). The top panel displays the amplitude profile of the lattice fields in the continuous (temporal) direction at the lattice sites belonging to "frame" (5) (the profile with the largest amplitude), and in two surrounding layers: At sites with $|m|=2, n=0$ and $m=0, |n|=2$ (the low profile with a slightly larger amplitude), and at sites with $|m|=|n|=1$ (the low profile with the smaller amplitude). The lattice distribution of the single-site energy, defined as per Eq. (21), is shown on the bottom panel by means of the hue-scale plot.

III. CROSS-VORTEX SOLITONS: NUMERICAL RESULTS

A. Stable vortices

To find numerical solutions corresponding to the semidiscrete solitons of the cross type, we used ansatz (11) as the starting point. Coefficients in the ansatz were taken as predicted by the VA, i.e., as per Eqs. (13), the single free parameter being μ. Then, systematic direct simulations of Eqs. (2) demonstrate that a stable cross- (rhombus-) shaped ("X") vortex soliton self-traps from the initial configuration with $\mu \ge \mu_{\rm cr}^{(\rm X)} \approx 19$ (the numerical analysis was extended up to $\mu=70$), while several distinct modes of instability are observed at $\mu < \mu_{\rm cr}$.

An example of the stable vortex found slightly above the stability threshold, viz., at $\mu=20$, is displayed in Fig. 1. The figure includes a set of temporal profiles of the soliton in the continuum direction, $|u_{mn}(\tau)|$, and a contour plot which

shows the transverse distribution (on the square grid) of the single-site energy integrated in the longitudinal direction,

$$E_{m,n} = \frac{1}{2}\int_{-\infty}^{+\infty} |u_{m,n}(\tau)|^2 d\tau. \tag{21}$$

Comparison of the VA predictions with the numerical findings demonstrates proximity between them. In particular, Eqs. (11) and (13) with $\mu=20$ predict the amplitude of the main component of the vortex, at sites belonging to "frame" (5),

$$A_{1,0}^{(\mathrm{X})} = \sqrt{2(4+\mu)} \approx 6.93, \tag{22}$$

and the amplitude in the next layer, at points with $|m|=2, n=0$ and $|n|=2, m=0$, to be

$$A_{2,0}^{(\mathrm{X})} = \sqrt{\frac{2}{4+\mu}} \approx 0.29. \tag{23}$$

The amplitude predicted by the VA in the layer with $|m|=|n|=1$ is

$$A_{1,1}^{(\mathrm{X})} = 1/\sqrt{4+\mu} = 1/(2\sqrt{6}) \approx 0.20. \tag{24}$$

As seen in Fig. 1, these values are indeed very close to their numerical counterparts, which can be evaluated as $A_{1,0}^{(\mathrm{X})} \approx 6.89$, $A_{2,0}^{(\mathrm{X})} \approx 0.20$, and $A_{1,1}^{(\mathrm{X})} \approx 0.28$. However, a minor discrepancy is seen in the fact that the numerically found amplitudes in the two secondary layers, $A_{2,0}^{(\mathrm{X})}$ and $A_{1,1}^{(\mathrm{X})}$, are exchanged with respect to the VA.

B. Instability scenarios

It is also interesting to consider various modes of the development of the instability for the cross vortices at $\mu<19$. This was done for $\mu \geq -3.5$ [Eqs. (7) and (13) suggest that the solutions may exist at $\mu>-4$]. First, in interval $-3.5<\mu\lesssim 1.8$, the initial pattern suffers straightforward decay (simultaneous diffraction and dispersion, in the transverse and longitudinal directions). More interesting dynamics is observed in the adjacent interval, $1.9\lesssim\mu\lesssim 4.3$, where the four components forming the initial vortex fuse into a single stable fundamental soliton, carried, essentially, by the central core, which was originally empty. A typical example of the fusion is displayed in Fig. 2 for $\mu=4.3$. It is seen that the fusion is preceded by some spontaneous (instability-induced) symmetry breaking of the field distribution on the vortex' frame. The nonconservation of the vorticity, evident in this case, is quite possible, as the model has no rotational invariance which would be necessary to make the vorticity a dynamical invariant.

Another outcome of the instability is observed in interval $5\lesssim\mu\lesssim 18$ (at larger μ, the cross vortex becomes stable, as said above): The symmetry between the four main original components of the vortex soliton is broken, and, while a small amount of energy is still transferred to the central core, the original pulses do not all vanish; starting from $\mu=5.5$, none of them vanishes. Simultaneously, the pulses separate in the longitudinal (temporal) direction, and lose mutual phase coherence, as shown in Figs. 3 and 4 (in fact, two

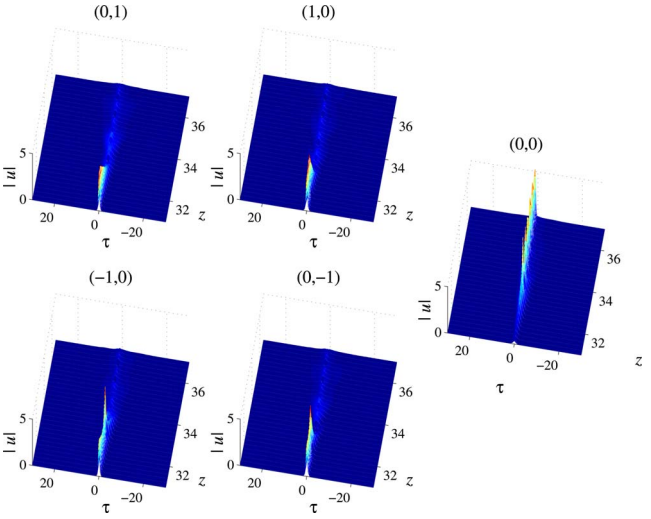

FIG. 2. (Color online) Fusion of the original cross-shaped vortex into a nearly single-component fundamental soliton, at $\mu=4.3$, is shown by means of evolution plots for the power, $|u_{m,n}(\tau)|^2$, at four sites that constitute the initial frame of the vortex, see Eq. (5), and at the central (originally empty) site.

pulses out of the four do not separate, and change the original phase difference between them, $\pi/2$, to 2π). Note that each pulse staying in the original frame is coupled to its counterpart in the central core.

IV. SQUARE-SHAPED VORTICES

A. Stable vortices

Vortices based on frame (8) were looked for in the numerical form, starting with the following initial ansatz [cf. Eq. (11)], which implies that the virtual center of the square-shaped vortex is set at the point with coordinates (0.5,0.5):

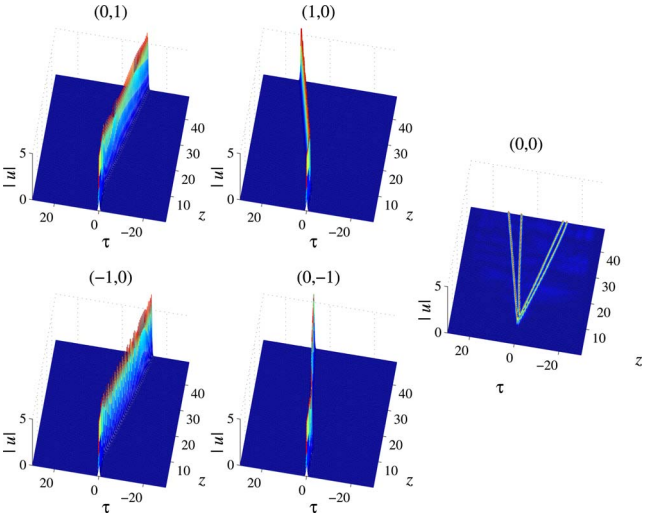

FIG. 3. (Color online) Splitting of an unstable vortex soliton at $\mu=18$ into individual pulses, each inducing a component in the central core.

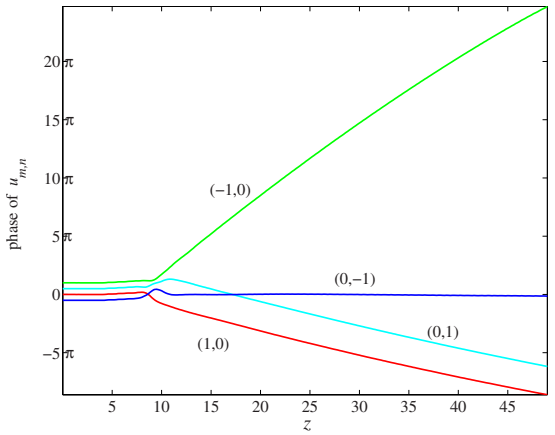

FIG. 4. (Color online) Evolution of the phases at the center of the individual components of the lattice fields shown in Fig. 3.

$$u_{mn}(\tau,0) = \sqrt{2}[(m-0.5)+i(n-0.5)] \times e^{-a(|m-0.5|+|n-0.5|-1)} \frac{\eta}{\cosh(\eta\tau)}. \quad (25)$$

Here we again take $\eta=\sqrt{2(4+\mu)}$ and $a=\ln[2(4+\mu)]$, cf. Eqs. (13). The simulations were performed in the range of $-3 \lesssim \mu \lesssim 300$. Unlike the cross- (rhombus-) shaped vortex, which was found to be stable in the semi-infinite region, $\mu \gtrsim 19$, the present species of the vortex soliton features stability in two disjoint finite intervals, $3 \lesssim \mu \lesssim 8$ and $20 \lesssim \mu \lesssim 22$ (it is not ruled out that extremely accurate numerical analysis could reveal additional very narrow stability windows, or subintervals of a very weak instability inside the stability regions). Examples of stable vortices found in the two regions are displayed in Figs. 5 and 6.

B. Instability

In cases when the square-shaped vortex solitons are unstable, their instability may feature development scenarios different from those presented above for the vortices of the cross or rhombus type. In particular, at $\mu=-3$, the original vortex quickly transforms itself, via an intermediate necklacelike pattern with four peaks, into a stable structure with two peaks, as shown in Fig. 7. In this case, an instability of the phase distribution starts to develop first in the initial vortex. The particular pair of surviving peaks may be selected by random noise which initiates the onset of the instability.

In interval $-1 \lesssim \mu \lesssim 2$, the square vortices are subject to straightforward decay. The character of the instability changes in region $9 \lesssim \mu \lesssim 19$: In this case, we chiefly observe splitting of the peaks in the longitudinal direction, roughly similar to what was observed above in Fig. 3. In addition, one of the peaks is often absorbed by the others, therefore in most cases the final state contains three far separated fundamental solitons, each carried, approximately, by a single core. After passing the second stability island, $20 \lesssim \mu \lesssim 22$, a similar splitting instability sets in again, and persists up to very large values of μ. In this case, the spontaneous symmetry breaking causes, chiefly, the emergence of four far separated fundamental solitons with different amplitudes. However, a single soliton survives at some values of μ (in particular, at $\mu=24$ and $\mu=300$), and in some other cases the eventual configuration may contain two (at $\mu=23$) or three peaks (the latter happens, for instance, at $\mu=25$ and $\mu=30$).

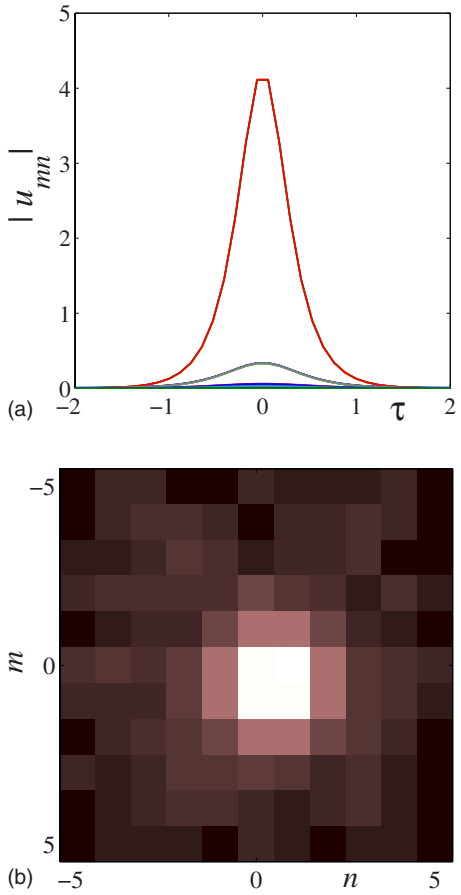

FIG. 5. (Color online) An example of a stable vortex soliton of the square type, which self-traps from initial configuration (25) with $\mu=5$ (stable vortex solitons of this type are generated in the region of $3 \lesssim \mu \lesssim 8$). The panels have the same meaning as in Fig. 1 [the top panel displays the field profiles at the lattice sites belonging to "frame" (8), and at the two next layers, corresponding to squared distances $1.5^2+0.5^2 \equiv 2.5$ and $1.5^2+1.5^2 \equiv 4.5$ from the center of the vortex].

V. VORTICES WITH CHARGE $S=2$

A. Rhombuses

The next natural step is to consider solitons with the double vorticity, $S=2$. In the case of the rhombus-shaped pattern (the name of "cross" is not appropriate in this case), a natural extension of initial ansatz (11) that features the necessary topological charge is

$$u_{mn}(t,0) = \frac{(m+in)^2 e^{-a||m|+|n|-2|}}{m^2+n^2} \frac{\eta}{\cosh(\eta t)}, \quad (26)$$

once again with $\eta=\sqrt{2(4+\mu)}$ and $a=\ln[2(4+\mu)]$, as suggested by the exact soliton solution for the single core. This ansatz features eight distinct peaks.

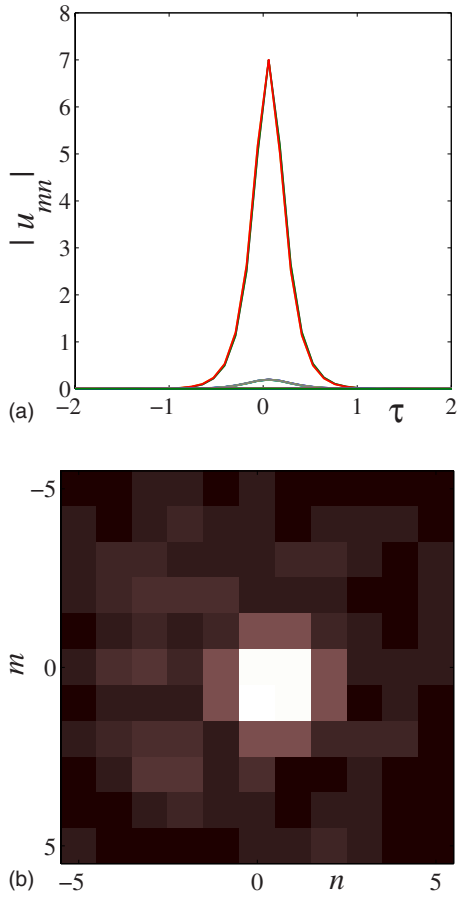

FIG. 6. (Color online) The same as in Fig. 5, but for $\mu=20$ (stable vortex solitons of this type are found in interval $20 \lesssim \mu \lesssim 22$).

Numerical results for this species of the vortex solitons were collected in the range of $-3 \lesssim \mu \lesssim 200$. In compliance with the known results for higher-order discrete vortices

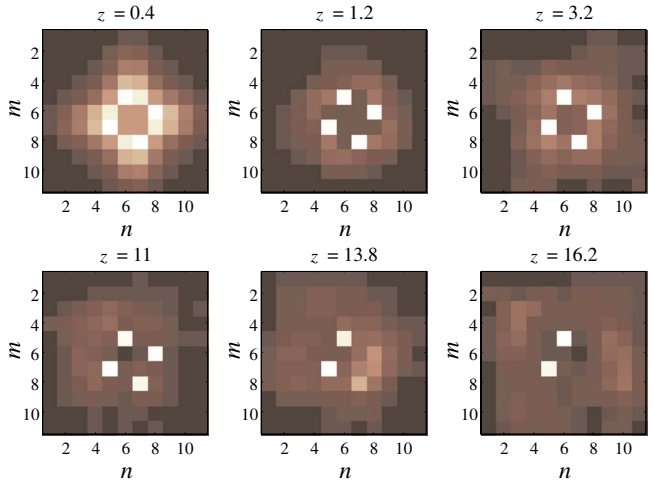

FIG. 7. (Color online) Evolution of the unstable vortex of the square type with $\mu=-3$, presented by means of the plots that show the distribution of the integrated single-site energy [see Eq. (21)] across the lattice, cf. bottom panels of Figs. 1, 5, and 6. The discrete coordinates are shifted here with respect to the notation adopted in Eq. (8).

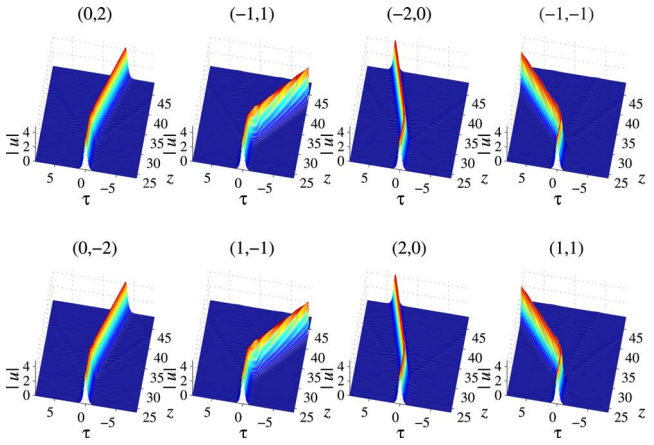

FIG. 8. (Color online) Splitting of the unstable rhombus-shaped vortex with $S=2$, via an intermediate stage of two quadrupoles, into a set of four solitons pairs, at $\mu=7$.

without the temporal dimension [8], the semidiscrete spatiotemporal vortices with $S=2$ are never stable. In particular, they directly decay in the simulations starting with $\mu \lesssim 1$. At $\mu \gtrsim 3$, two successive instabilities are observed. First, the eight-peak vortex transforms itself into a pair of copropagating quadrupoles, which are not phase correlated with each other (at $\mu \lesssim 25$, the transition to the quadrupoles is smooth, while at larger μ it becomes sharp). However, the emerging quadrupoles are unstable too. In particular, at $\mu=3$ and 5, they further merge into just two fundamental (essentially, single-core) solitons. At $\mu=7$, another outcome is observed: The quadrupole pair splits into a set of four soliton pairs. While the pairs separate, each of them keeps zero temporal distance and zero phase shift between the constituent solitons, see Fig. 8. Further, in the interval of $11 \lesssim \mu \lesssim 20$, the pattern splits into eight uncorrelated slowly separating fundamental solitons.

A surprising outcome of the evolution of the vortex of the rhombus type with $S=2$ is observed at $\mu \gtrsim 25$: The phase coherence between the eight constituent solitons is completely washed out, but their temporal (longitudinal) positions remain locked, as shown in Fig. 9 (as long as the simulations were run—at least, up to the propagation distance corresponding to $z=29$, in the present notation). A possible explanation to this phenomenon is that, for sufficiently large μ, the constituent solitons become too heavy [their effective mass is $2\eta \approx 2\sqrt{2(4+\mu)}$], hence the relatively weak linear interaction between them cannot generate sufficient momentum to initiate the separation between these solitons.

B. Squares

We also considered vortex solitons of the square type with $S=2$, which too are built of eight peaks. It has been concluded that this species of the vortex cannot be stable either. Similar to what was presented in some detail above for the rhombus-shaped vortices with $S=2$, their counterparts of the square type tend, at first, to split into two quadrupoles, which too turn out to be unstable. Unless the pattern completely decays (which happens at $\mu \lesssim 1$), the quadrupoles eventually

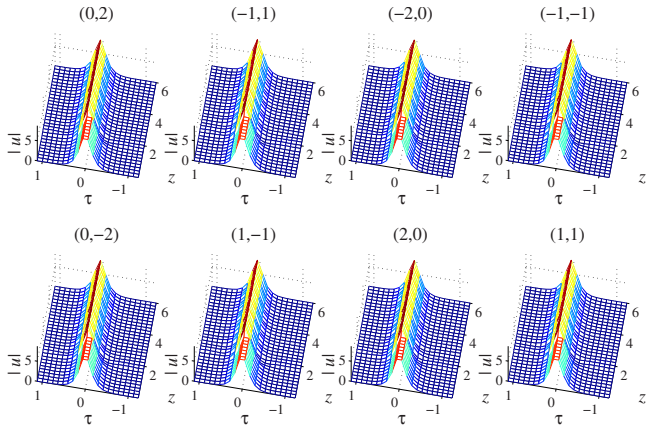

FIG. 9. (Color online) Transformation of the unstable rhombus-shaped vortex with $S=2$ and $\mu=30$ into a set of eight mutually incoherent solitons, which, however, keep their positions locked together. The sudden disruption in the initial evolution at $z\approx 1.6$ signalizes the transformation of the vortex into two quadrupoles, which is gradually followed by the loss of the coherence between the individual solitons. A qualitatively similar outcome of the evolution of the unstable vortices of the rhombus type with $S=2$ is observed for all $\mu\geq 25$.

split into several mutually incoherent separating fundamental solitons. The final number of the "splinters" varies from 1 to 8. They may have different amplitudes and velocities, and their trajectories in the (z,t) plane may be different from straight lines. In particular, at $\mu=3$ all peaks, except for the ones located at sites (1,0) and (0,1), are absorbed into these two peaks, which is followed by their fusion into a single fundamental soliton at the central site. Further, the number of the surviving disconnected fundamental solitons is, typically, two to four for $5\lesssim\mu\lesssim 11$, and six or seven for $15\lesssim\mu\lesssim 30$, increasing to the maximum, eight, for $50\lesssim\mu\lesssim 200$. However, only three splinters survive at $\mu=300$. Depending on μ, the peaks may separate (and lose their phase correlations) slower or faster (for instance, the separation is delayed at $\mu=5,7$, and 11).

VI. QUADRUPOLES

Although the quadrupole solitons carry no vorticity, they are akin to the vortices with $S=2$ [8]. As suggested by variational ansatz (17) and Eqs. (19), we used the following initial configuration, to explore the dynamics of the quadrupoles:

$$u_{mn}(t,0)=\eta\frac{(m^2-n^2)e^{-a(|m|+|n|-1)}}{\cosh\ \eta t}, \tag{27}$$

with $\eta=\sqrt{2(4+\mu)}$ and $a=\ln[2(4+\mu)]$, as before. Note that, being built around frame (5), the quadrupole includes four main peaks (unlike the $S=2$ vortices which feature eight peaks). Numerical data for the quadrupole solitons were collected in the range of $-3\lesssim\mu\lesssim 70$.

The most important finding is that, similar to the situation of the lattice solitons without the longitudinal direction, the quadrupoles may be stable, while all vortices with $S=2$, of either type (rhombuses or squares), are completely unstable.

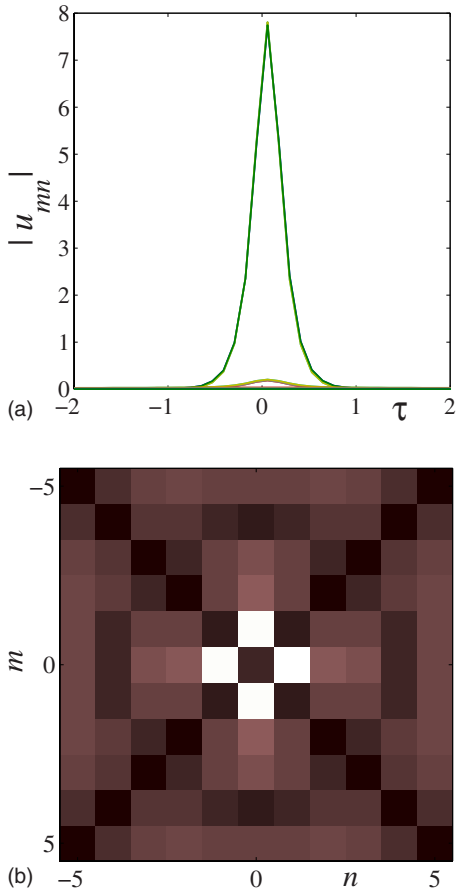

FIG. 10. (Color online) An example of a stable quadrupole soliton, which self-traps form initial configuration (27) with $\mu=25$ (the quadrupoles are stable for $\mu\geq 20$). The panels have the same meaning as in Fig. 1 [the top panel displays the field profiles at the lattice sites belonging to "frame" (5), and in the next layer, formed by the sites with $|m|=2,n=0$ and $m=0,|n|=2$].

The stability region for the quadrupoles is $\mu\geq\mu_{\rm cr}^{(\rm Q)}\approx 20$ (note that it is quite close to the stability threshold $\mu_{\rm cr}^{(\rm X)}\approx 19$ for the cross-shaped vortices with $S=1$, see above). A typical example of a stable stationary quadrupole is displayed in Fig. 10.

Note that the VA, i.e., Eqs. (17) and (19), predict the following amplitudes of the quadrupole's component at sites belonging to the frame and to the next layer, for $\mu=25$,

$$A_{1,0}^{(\rm Q)}=\sqrt{2(4+\mu)}\approx 7.62,\quad A_{2,0}^{(\rm Q)}=\frac{3}{2\sqrt{2(4+\mu)}}\approx 0.20, \tag{28}$$

cf. Eqs. (22) and (23). Values (28) are in a quite reasonable agreement with the numerical results presented in Fig. 10: $A_{1,0}^{(\rm Q)}\approx 7.77$ and $A_{2,0}^{(\rm Q)}\approx 0.17$.

The dynamics of unstable quadrupole solitons with $\mu<20$ was investigated too. It has been found that the soliton completely decays at $\mu<1$, while at values of μ close to 1 the quadrupole merges into a single fundamental soliton, transferring almost all the energy into the central point, see Fig. 11. Qualitatively, the merger is similar to what was seen

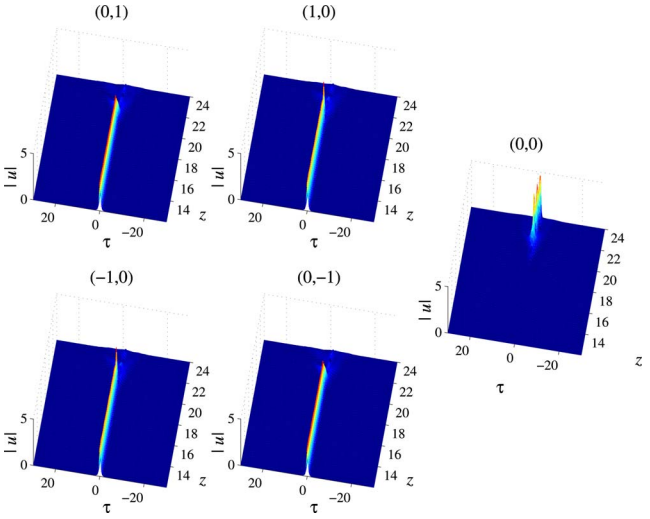

FIG. 11. (Color online) Fusion of the unstable quadrupole into a single-component fundamental soliton, at $\mu=1$, cf. Fig. 2 for the fusion of the unstable cross-shaped vortex with $S=1$.

above in Fig. 2 for the unstable cross-shaped vortex, but an essential difference is that, in the present case, the instability develops much slower, demonstrating the trend of the quadrupole to be a robust object [in fact, the decay of the quadrupole at $\mu<1$ (not shown here) is also much slower than the decay of unstable vortices].

At larger values of μ, up to the stability threshold at $\mu \approx 20$, the generic instability scenario amounts to splitting of the quadrupole into two stable or quasistable (see below) pairs of in-phase fundamental solitons, which maintain zero separation (in the longitudinal direction) in each pair. An example of the splitting is displayed in Fig. 12, for $\mu=5$. It may be concluded that the effect is similar to that shown above in Fig. 3 for the unstable cross or rhombus vortex, but, as well as in the case of the fusion, the instability development is much slower in the case of the quadrupole. A modification of this scenario, observed in interval $12 \lesssim \mu \lesssim 19$, is that one of the emerging pairs may eventually split into individual solitons, after passing quite a long distance (roughly, 2 times that which was necessary for the primary splitting of the quadrupole into two soliton pairs).

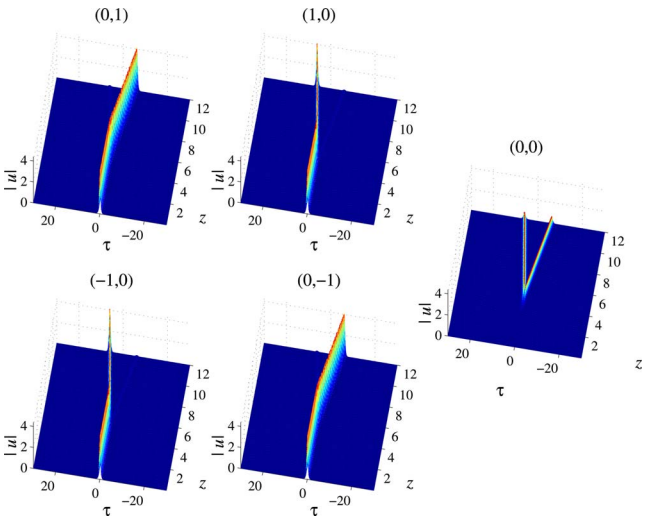

FIG. 12. (Color online) Splitting of the unstable quadrupole into two stable in-phase soliton pairs, at $\mu=5$ [cf. the splitting of the unstable cross- (rhombus-) shaped vortex into pairs, shown in Fig. 3].

VII. CONCLUSION

The aim of this work is to introduce several species of complex spatiotemporal solitons in the model describing a bundled set of nonlinear optical fibers; the medium is actually available to the experiment, in the form of a set of parallel waveguides written in bulk silica [11,12]. The creation of spatiotemporal solitons in this setting may be possible under experimental conditions similar to those that allow the formation of 2D discrete solitons [11], if a pulsed laser beam is used as a source, with the pulse duration in the femtosecond range. The same model applies to a BEC trapped in a very strong quasi-2D optical lattice, in the 3D space.

The solitons that were considered in this work are continuous in the longitudinal (temporal) direction, and represent discrete structures in the transverse plane. By means of the VA (variational approximation) and direct numerical methods, we have studied several families of semidiscrete solitons, including two species of vortices (crosses or rhombuses and squares) with topological charge $S=1$ and 2, and quadrupoles. The VA was developed for the cross-shaped vortices ("X") with $S=1$, and for the quadrupoles ("Q"). These are two soliton species with the biggest stability regions—they are stable if propagation constant μ exceeds a critical value, which is nearly the same for both species, $\mu_{\rm cr}^{(\rm X)} \approx 19$ and $\mu_{\rm cr}^{(\rm Q)} \approx 20$, respectively. Generally, the quadrupole solitons tend to be very robust objects; in particular, when they are unstable, the instability develops very slowly. For the square-shaped vortices with $S=1$, two finite stability intervals were found, $3 \lesssim \mu \lesssim 8$ and $20 \lesssim \mu \lesssim 22$, whereas all vortices with $S=2$ are unstable, as in the ordinary DNLS equation in two dimensions [8]. Note, however, that spatiotemporal vortex solitons with $S=2$ may be stable in the continuous counterpart of the present model, i.e., the 3D continuous NLS equation with the self-focusing nonlinearity and quasi-2D periodic potential [31] (see also Ref. [42]).

For the unstable soliton species, various scenarios of the instability development were identified, that include straightforward decay, merger of the complex semidiscrete localized pattern into a single fundamental soliton, or splitting into several mutually incoherent fundamental solitons, each carried, essentially, by a single core. In some cases, the eventual state may include stable coherent pairs of in-phase solitons. In particular, the latter outcome is characteristic to the instability of quadrupoles.

The model analyzed in the paper can be developed in various directions. First, one may try to construct spatiotemporal semidiscrete vortex solitons with $S=3$, which probably may be stable. A straightforward extension would be to consider collisions between the spatiotemporal solitons moving

in the longitudinal direction. It could also be interesting to consider spatiotemporal solitons, including vortices, in a model of a twisted fiber bundle. Very recently, discrete 2D fundamental and vortical solitons were studied in a 2D lattice model including the twist [43].

ACKNOWLEDGMENT

One of the authors (B.A.M.) appreciates the hospitality of Laboratoire POMA at Université d'Angers (Angers, France).

[1] P. G. Kevrekidis, K. Ø. Rasmussen, and A. R. Bishop, Int. J. Mod. Phys. B **15**, 2833 (2001).

[2] D. N. Christodoulides and R. I. Joseph, Opt. Lett. **13**, 794 (1988).

[3] H. S. Eisenberg, Y. Silberberg, R. Morandotti, A. R. Boyd, and J. S. Aitchison, Phys. Rev. Lett. **81**, 3383 (1998); D. N. Christodoulides, F. Lederer, and Y. Silberberg, Nature (London) **424**, 817 (2003); T. Pertsch, U. Peschel, J. Kobelke, K. Schuster, H. Bartelt, S. Nolte, A. Tünnermann, and F. Lederer, *ibid.* **93**, 053901 (2004).

[4] N. K. Efremidis, S. Sears, D. N. Christodoulides, J. W. Fleischer, and M. Segev, Phys. Rev. E **66**, 046602 (2002); N. K. Efremidis, J. Hudock, D. N. Christodoulides, J. W. Fleischer, O. Cohen, and M. Segev, Phys. Rev. Lett. **91**, 213906 (2003); J. W. Fleischer, G. Bartal, O. Cohen, T. Schwartz, O. Manela, B. Freedman, M. Segev, H. Buljan, and N. K. Efremidis, Opt. Express **13**, 1780 (2005).

[5] J. W. Fleischer, M. Segev, N. K. Efremidis, and D. N. Christodoulides, Nature (London) **422**, 147 (2003); J. W. Fleischer, G. Bartal, O. Cohen, O. Manela, M. Segev, J. Hudock, and D. N. Christodoulides, Phys. Rev. Lett. **92**, 123904 (2004).

[6] D. Neshev, T. Alexander, E. Ostrovskaya, Y. S. Kivshar, H. Martin, I. Makasyuk, and Z. Chen, Phys. Rev. Lett. **92**, 123903 (2004); J. W. Fleischer, G. Bartal, O. Cohen, O. Manela, M. Segev, J. Hudock, and D. N. Christodoulides, *ibid.* **92**, 123904 (2004).

[7] B. A. Malomed and P. G. Kevrekidis, Phys. Rev. E **64**, 026601 (2001).

[8] P. G. Kevrekidis, B. A. Malomed, Z. Chen, and D. J. Frantzeskakis, Phys. Rev. E **70**, 056612 (2004).

[9] O. Manela, O. Cohen, G. Bartal, J. W. Fleischer, and M. Segev, Opt. Lett. **29**, 2049 (2004).

[10] J. Yang, I. Makasyuk, P. G. Kevrekidis, H. Martin, B. A. Malomed, D. J. Frantzeskakis, and Z. Chen, Phys. Rev. Lett. **94**, 113902 (2005).

[11] A. Szameit, J. Burghoff, T. Pertsch, S. Nolte, A. Tünnermann, and F. Lederer, Opt. Express **14**, 6055 (2006); A. Szameit, T. Pertsch, F. Dreisow, S. Nolte, A. Tünnermann, U. Peschel, and F. Lederer, Phys. Rev. A **75**, 053814 (2007).

[12] T. Pertsch, U. Peschel, F. Lederer, J. Burghoff, M. Will, S. Nolte, and A. Tünnermann, Opt. Lett. **29**, 468 (2004); A. Szameit, D. Blömer, J. Burghoff, T. Schreiber, T. Pertsch, S. Nolte, A. Tünnermann, and F. Lederer, Opt. Express **13**, 10552 (2005).

[13] P. Xie, Z.-Q. Zhang, and X. Zhang, Phys. Rev. E **67**, 026607 (2003); A. Ferrando, M. Zacarés, P. F. de Cordoba, D. Binosi, and J. A. Monsoriu, Opt. Express **11**, 452 (2003); A. Ferrando, M. Zacarés, P. F. de Cordoba, D. Binosi, and J. A. Monsoriu, *ibid.* **12**, 817 (2004); A. Ferrando, M. Zacarés, and M. A. García-March, Phys. Rev. Lett. **95**, 043901 (2005).

[14] M. J. Ablowitz, Z. H. Musslimani, and G. Biondini, Phys. Rev. E **65**, 026602 (2002).

[15] I. E. Papacharalampous, P. G. Kevrekidis, B. A. Malomed, and D. J. Frantzeskakis, Phys. Rev. E **68**, 046604 (2003).

[16] J. Meier, G. I. Stegeman, Y. Silberberg, R. Morandotti, and J. S. Aitchison, Phys. Rev. Lett. **93**, 093903 (2004); J. Meier, G. I. Stegeman, D. N. Christodoulides, R. Morandotti, M. Sorel, H. Yang, G. Salamo, J. S. Aitchison, and Y. Silberberg, Opt. Express **13**, 1797 (2005); Y. Linzon, Y. Sivan, B. Malomed, M. Zaezjev, R. Morandotti, and S. Bar-Ad, Phys. Rev. Lett. **97**, 193901 (2006).

[17] D. Cheskis, S. Bar-Ad, R. Morandotti, J. S. Aitchison, H. S. Eisenberg, Y. Silberberg, and D. Ross, Phys. Rev. Lett. **91**, 223901 (2003).

[18] A. Trombettoni and A. Smerzi, Phys. Rev. Lett. **86**, 2353 (2001); G. L. Alfimov, P. G. Kevrekidis, V. V. Konotop, and M. Salerno, Phys. Rev. E **66**, 046608 (2002); R. Carretero-González and K. Promislow, Phys. Rev. A **66**, 033610 (2002); F. S. Cataliotti, S. Burger, C. Fort, P. Maddaloni, F. Minardi, A. Trombettoni, A. Smerzi, and M. Inguscio, Science **293**, 843 (2001); M. Greiner, O. Mandel, T. Esslinger, T. W. Hänsch, and I. Bloch, Nature (London) **415**, 39 (2002); N. K. Efremidis and D. N. Christodoulides, Phys. Rev. A **67**, 063608 (2003); M. A. Porter, R. Carretero-González, P. G. Kevrekidis, and B. A. Malomed, Chaos **15**, 015115 (2005).

[19] J. E. Heebner and R. W. Boyd, J. Mod. Opt. **49**, 2629 (2002); P. Chak, J. E. Sipe, and S. Pereira, Opt. Lett. **28**, 1966 (2003); J. J. Baumberg, P. G. Savvidis, R. M. Stevenson, A. I. Tartakovskii, M. S. Skolnick, D. M. Whittaker, and J. S. Roberts, Phys. Rev. B **62**, R16247 (2000); P. G. Savvidis and P. G. Lagoudakis, Semicond. Sci. Technol. **18**, S311 (2003).

[20] A. B. Aceves, C. De Angelis, A. M. Rubenchik, and S. K. Turitsyn, Opt. Lett. **19**, 329 (1994); A. V. Buryak and N. N. Akhmediev, IEEE J. Quantum Electron. **31**, 682 (1995).

[21] A. B. Aceves, G. G. Luther, C. De Angelis, A. M. Rubenchik, and S. K. Turitsyn, Phys. Rev. Lett. **75**, 73 (1995).

[22] A. B. Aceves, C. De Angelis, T. Peschel, R. Muschall, F. Lederer, S. Trillo, and S. Wabnitz, Phys. Rev. E **53**, 1172 (1996); A. B. Aceves and M. Santagiustina, *ibid.* **56**, 1113 (1997).

[23] A. B. Aceves, C. De Angelis, G. G. Luther, and A. M. Rubenchik, Opt. Lett. **19**, 1186 (1994); E. W. Laedke, K. H. Spatschek, S. K. Turitsyn, and V. K. Mezentsev, Phys. Rev. E **52**, 5549 (1995); S. Darmanyan, I. Relke, and F. Lederer, *ibid.* **55**, 7662 (1997); A. B. Aceves, M. Santagiustina, and C. De Angelis, J. Opt. Soc. Am. B **14**, 1807 (1997); I. Relke, Phys. Rev. E **57**, 6105 (1998); M. Stepić, L. Hadžievski, and M. M. Skorić, *ibid.* **65**, 026604 (2002); A. V. Yulin, D. V. Skryabin, and A. G. Vladimirov, Opt. Express **14**, 12347 (2006).

[24] B. A. Malomed, D. Mihalache, F. Wise, and L. Torner, J. Opt.

B: Quantum Semiclassical Opt. **7**, R53 (2005).
[25] Z. Y. Xu, Y. V. Kartashov, L. C. Crasovan, D. Mihalache, and L. Torner, Phys. Rev. E **70**, 066618 (2004); N. C. Panoiu, R. M. Osgood, and B. A. Malomed, Opt. Lett. **31**, 1097 (2006).
[26] D. Mihalache, D. Mazilu, F. Lederer, and Y. S. Kivshar, Opt. Express **15**, 589 (2007); D. Mihalache, D. Mazilu, Y. S. Kivshar, and F. Lederer, *ibid.* **15**, 10718 (2007).
[27] D. Mihalache, D. Mazilu, F. Lederer, and Y. S. Kivshar, Opt. Lett. **32**, 2091 (2007).
[28] M. I. Molina and Y. S. Kivshar, Phys. Lett. A **362**, 280 (2007).
[29] D. Mihalache, D. Mazilu, F. Lederer, and Y. S. Kivshar, Opt. Lett. **32**, 3173 (2007).
[30] B. B. Baizakov, B. A. Malomed, and M. Salerno, Phys. Rev. A **70**, 053613 (2004); D. Mihalache, D. Mazilu, F. Lederer, Y. V. Kartashov, L.-C. Crasovan, and L. Torner, Phys. Rev. E **70**, 055603(R) (2004).
[31] H. Leblond, B. A. Malomed, and D. Mihalache, Phys. Rev. E **76**, 026604 (2007).
[32] P. G. Kevrekidis, B. A. Malomed, D. J. Frantzeskakis, and R. Carretero-González, Phys. Rev. Lett. **93**, 080403 (2004); R. Carretero-González, P. G. Kevrekidis, B. A. Malomed, and D. J. Frantzeskakis, *ibid.* **94**, 203901 (2005).
[33] G. P. Agrawal, *Nonlinear Fiber Optics* (Academic, San Diego, 1995).
[34] D. V. Petrov, F. Canal, and L. Torner, Opt. Commun. **143**, 265 (1997); D. V. Petrov, L. Torner, J. Martorell, R. Vilaseca, J. P. Torres, and C. Cojocaru, Opt. Lett. **23**, 1444 (1998).
[35] K. P. Marzlin, W. P. Zhang, and E. M. Wright, Phys. Rev. Lett. **79**, 4728 (1997); R. Dum, J. I. Cirac, M. Lewenstein, and P. Zoller, *ibid.* **80**, 2972 (1998); L. Dobrek, M. Gajda, M. Lewenstein, K. Sengstock, G. Birkl, and W. Ertmer, Phys. Rev. A **60**, R3381 (1999).
[36] K. W. Madison, F. Chevy, W. Wohlleben, and J. Dalibard, Phys. Rev. Lett. **84**, 806 (2000); S. Inouye, S. Gupta, T. Rosenband, A. P. Chikkatur, A. Gorlitz, T. L. Gustavson, A. E. Leanhardt, D. E. Pritchard, and W. Ketterle, *ibid.* **87**, 080402 (2001); C. Raman, J. R. Abo-Shaeer, J. M. Vogels, K. Xu, and W. Ketterle, *ibid.* **87**, 210402 (2001).
[37] R. Driben, B. A. Malomed, A. Gubeskys, and J. Zyss, Phys. Rev. E **76**, 066604 (2007).
[38] B. A. Malomed and M. I. Weinstein, Phys. Lett. A **220**, 91 (1996); R. Carretero-González, J. D. Talley, C. Chong, and B. A. Malomed, Physica D **216**, 77 (2006).
[39] M. I. Weinstein, Nonlinearity **12**, 673 (1999).
[40] N. G. Vakhitov and A. A. Kolokolov, Izv. Vyssh. Uchebn. Zaved., Radiofiz. **16**, 1020 (1973) [Radiophys. Quantum Electron. **16**, 783 (1973)].
[41] L. Bergé, Phys. Rep. **303**, 259 (1998).
[42] H. Sakaguchi and B. A. Malomed, Europhys. Lett. **72**, 698 (2005).
[43] J. Cuevas, B. A. Malomed, and P. G. Kevrekidis, Phys. Rev. E **76**, 046608 (2007).